JOURNAL OF GLACIOLOGY

CAMBRIDGE UNIVERSITY PRESS

Subglacial hydrology modeling predicts high winter water pressure and spatially variable transmissivity at Helheim Glacier, Greenland

Journal:	*Journal of Glaciology*
Manuscript ID	Draft
Manuscript Type:	Article
Date Submitted by the Author:	n/a
Complete List of Authors:	Sommers, Aleah; Dartmouth College, Thayer School of Engineering Meyer, Colin; Dartmouth College Morlighem, Mathieu; Dartmouth College, Department of Earth Sciences Rajaram, Harihar; Johns Hopkins University Poinar, Kristin; University at Buffalo, Geology Chu, Winnie; Georgia Institute of Technology Mejia, Jessica; University at Buffalo, Geosciences
Keywords:	Subglacial processes, Glacier hydrology, Ice-sheet modelling, Glacier modelling, Melt - basal
Abstract:	Sliding velocity of glaciers is influenced by water pressure at the bed. Subglacial hydrology models are helpful for gaining insight into basal conditions, but models depend on several unconstrained physical parameters, and reproducing elevated water pressures in winter has been a challenge. We eliminate terms in the SHAKTI model that rely on uncertain parameters and apply this model to Helheim Glacier in east

Greenland to explore the winter base state of the subglacial drainage system in the absence of meltwater inputs from the surface. Our results suggest that meltwater produced at the bed alone can support an active winter drainage system at Helheim. We produce large areas of elevated water pressure and naturally emerging preferential drainage pathways, with a continuum approach that allows for transitions between flow regimes and drainage system opening by melt. Transmissivity varies spatially over several orders of magnitude, including large regions of weak transmissivity, representing poorly connected regions of the system. Deeply incised bed topography controls the location of primary drainage pathways, with high basal melt rates along the steep walls. We examine the influence of frictional heat from sliding by comparing simulations with three different approaches for calculating basal shear stress.

Journal of Glaciology, Vol. 00, No. 0, 0000 1

Subglacial hydrology modeling predicts high winter water pressure and spatially variable transmissivity at Helheim Glacier, Greenland

Aleah SOMMERS,[1] Colin MEYER,[1] Mathieu MORLIGHEM,[1] Harihar RAJARAM,[2] Kristin POINAR,[3] Winnie CHU,[4] Jessica MEJIA[3]

[1]*Dartmouth College, Hanover, NH, USA*

[2]*Johns Hopkins University, Baltimore, MD, USA*

[3]*University at Buffalo, Buffalo, NY, USA*

[4]*Georgia Institute of Technology, Atlanta, GA, USA*

Correspondence: Aleah Sommers <Aleah.N.Sommers@dartmouth.edu>

ABSTRACT. Sliding velocity of glaciers is influenced by water pressure at the bed. Subglacial hydrology models are helpful for gaining insight into basal conditions, but models depend on several unconstrained physical parameters, and reproducing elevated water pressures in winter has been a challenge. We eliminate terms in the SHAKTI model that rely on uncertain parameters and apply this model to Helheim Glacier in east Greenland to explore the winter base state of the subglacial drainage system in the absence of meltwater inputs from the surface. Our results suggest that meltwater produced at the bed alone can support an active winter drainage system at Helheim. We produce large areas of elevated water pressure and naturally emerging preferential drainage pathways, with a continuum approach that allows for transitions between flow regimes and drainage system opening by melt. Transmissivity varies spatially over several orders of magnitude, including large regions of weak transmissivity, representing poorly connected regions of the system. Deeply incised bed topography controls the location of primary drainage pathways, with high basal melt rates along the steep walls. We examine the influence of frictional heat from sliding by comparing simulations with three different approaches

for calculating basal shear stress.

INTRODUCTION

Conditions at the bed of ice sheets and glaciers strongly influence ice dynamics through the effect of lubrication and enhanced sliding where basal water pressure is high. Unfortunately, direct observations are difficult to obtain beneath hundreds to thousands of meters of ice. Techniques such as drilling boreholes to the bed (Iken and others, 1993; Murray and Clarke, 1995; Harper and others, 2005; Fudge and others, 2008; Ryser and others, 2014b; Andrews and others, 2014), using radar sounding to infer the presence of liquid basal water (Oswald and Gogineni, 2008; Chu and others, 2016; Jordan and others, 2018; Oswald and others, 2018), and dye-tracing tests (Nienow and others, 1998; Cowton and others, 2013) are helpful means to gain a view into basal conditions, but do not provide a complete description of the spatially and temporally heterogeneous bed environment.

Several numerical models have been developed to simulate the flow and pressure of water beneath glaciers and ice sheets (e.g., Flowers, 2015; de Fleurian and others, 2018) and have successfully reproduced melt-season drainage system evolution. However, challenges remain in these efforts, and subglacial hydrology model development remains an active area of research. One persistent issue is that many models rely on unconstrained parameters, for example, prescribing a typical height and spacing of asperities at the bed, or specifying hydraulic conductivity of drainage system components. Subglacial hydrology models are sensitive to these uncertain parameters, with small changes leading to substantial differences in simulated basal water pressures and drainage regimes (Werder and others, 2013; Banwell and others, 2016).

Another challenge is that models have had difficulty reproducing widespread areas of high winter water pressures (Flowers, 2015) that have been observed in Greenland borehole arrays (Harper and others, 2005; Ryser and others, 2014a). Recent work highlighting the importance of hydraulically disconnected regions of the bed and incorporating a representation of these isolated areas into drainage models has helped to explain this phenomenon (Hoffman and others, 2016; Rada and Schoof, 2018, 2019), linking disconnected regions with other drainage components that represent flow through inefficient sheet-like configurations and efficient channels. Different drainage “modes” are treated with disparate equations to represent distinct physical processes (for example, channels open by melting while the sheet-like system opens by sliding over asperities in the bed). However, distinguishing between drainage “modes” by applying separate equations to different portions of the bed imposes an artificial distinction and may fail to fully capture the continuum of spatio-temporally evolving drainage behavior that exists in reality.

In this paper, we describe a reduced form of the Subglacial Hydrology And Kinetic, Transient Interactions (SHAKTI) model to address the above-mentioned issues. First presented by Sommers and others (2018), SHAKTI takes a continuum approach without explicitly distinguishing between different drainage components, yet does represent behavior corresponding to different "modes" of drainage, primarily facilitated through flow regime transitions with a single set of equations. Here, we eliminate some terms that rely on unconstrained parameters or are otherwise physically problematic. After summarizing the equations governing the evolution of the subglacial hydrology system in SHAKTI, we apply the model to Helheim Glacier in east Greenland under winter conditions to demonstrate its capabilities in a real glacial setting and attempt to reconcile the outstanding problem of simulating high winter water pressures with a continuum model.

MODEL DESCRIPTION

Summary of equations

SHAKTI uses a single set of equations to calculate hydraulic head, effective pressure, basal water flux, and geometry of the subglacial drainage system. In contrast to other subglacial hydrology models, SHAKTI allows for natural transitions between laminar and turbulent flow, allowing distinct flow regimes to coexist in different regions of the model domain with spatially and temporally variable transmissivity, giving rise to a spectrum of inefficient and efficient drainage configurations. SHAKTI includes heat generated by energy dissipation within the water flow and opening of the drainage system by melt across the entire domain, unlike models that treat "inefficient" sheet-like and "efficient" channel-like components of the drainage system with different equations. SHAKTI's unified approach leads to the emergence and disappearance of flexible drainage configurations over time, conserving mass and energy within the system. In what follows, we summarize the original SHAKTI model equations, along with key modifications to eliminate terms that depend on unconstrained parameters. Whereas in the original SHAKTI formulation, we included terms to facilitate direct comparison to other models (de Fleurian and others, 2018), here we examine the model capabilities in the absence of these unconstrained terms. We note that evaluating behavior resulting from simulations with different terms removed is valuable because it allows us to attribute different outcomes in the simulation to the physical processes that we model. Tables 1 and 2 serve as convenient references for

Table 1. Variables

Symbol	Units	Description
b	m	Gap height
b_e	m	Englacial storage per unit area of bed
h	m	Hydraulic head
K	$\mathrm{m^2\ s^{-1}}$	Hydraulic transmissivity,
		$K = b^3 g/(12\nu(1+\omega Re))$
$\dot{m}$	$\mathrm{kg\ m^{-2}\ s^{-1}}$	Subglacial melt rate
N	Pa	Effective pressure, $N = p_i - p_w$
p_i	Pa	Ice overburden pressure, $p_i = \rho_i g H$
p_w	Pa	Water pressure, $p_w = \rho_w g(h - z_b)$
$\mathbf{q}$	$\mathrm{m^2\ s^{-1}}$	Water flux
Re	Dimensionless	Reynolds number, Re=$\lvert q\rvert/\nu$
t	s	Time
β	Dimensionless	Parameter controlling opening
		due to sliding over bed bumps,
		$\beta = (b_r - b)/l_r$ for $b < b_r$,
		$\beta = 0$ for $\beta \geqslant b_r$
τ_b	Pa	Basal stress
		$\tau_b = C^2 N \lvert\mathbf{u_b}\rvert$

the variables, constants, and parameters used in the equations. For a complete description of the original SHAKTI model, we refer readers to Sommers and others (2018).

SHAKTI is composed of partial differential equations that describe conservation of ice and water mass, drainage configuration, water flux, and internal melt generation. The water balance equation is written as

$$\frac{\partial b}{\partial t} + \frac{\partial b_e}{\partial t} + \nabla \cdot \mathbf{q} = \frac{\dot{m}}{\rho_w} + i_{e\rightarrow b}, \tag{1}$$

where b is the gap height between the ice and bed, b_e refers to a volume of water stored englacially per unit area of the bed, $\mathbf{q}$ is gap-integrated water flux through the subglacial system, $\dot{m}$ is the melt rate expressed as a mass flux (units of kg $\mathrm{m^{-2}\ s^{-1}}$), ρ_w is density of water, and $i_{e\rightarrow b}$ is the rate of meltwater input from the englacial system to the bed, which can be specified and handled by the model as a combination of distributed input (units of m $\mathrm{s^{-1}}$) and point inputs to represent moulins or crevasses (units of $\mathrm{m^3\ s^{-1}}$).

Table 2. Constants and parameters used in this study

Symbol	Value	Units	Description
A	2.4×10^{-24}	$\mathrm{Pa}^{-3}\ \mathrm{s}^{-1}$	Flow law parameter (for ice at 0° Celsius)
b_r	0	m	Typical height of bed bumps
C	Spatially varying	$\mathrm{s}^{1/2}\ \mathrm{m}^{-1/2}$	Drag coefficient used in basal stress calculation
c_t	7.5×10^{-8}	$\mathrm{K\ Pa}^{-1}$	Change of pressure melting point with temperature
c_w	4.22×10^{3}	$\mathrm{J\ kg}^{-1}\ \mathrm{K}^{-1}$	Heat capacity of water
G	0.05	$\mathrm{W\ m}^{-2}$	Geothermal flux
g	9.81	$\mathrm{m\ s}^{-2}$	Gravitational acceleration
H	Varying	m	Ice thickness (Morlighem and others, 2017)
$i_{e\to b}$	0	$\mathrm{m\ s}^{-1}$ or $\mathrm{m}^3\ \mathrm{s}^{-1}$	Input rate of meltwater from englacial system to subglacial system
L	3.34×10^{5}	$\mathrm{J\ kg}^{-1}$	Latent heat of fusion of water
l_r	0	m	Typical spacing between bed bumps
n	3	Dimensionless	Flow law exponent
$\mathbf{u}_b$	Varying	$\mathrm{m\ s}^{-1}$	Ice velocity (Joughin and others, 2018)
z_b	Varying	m	Bed elevation with respect to sea level (Morlighem and others, 2017)
ν	1.787×10^{-6}	$\mathrm{m}^2\ \mathrm{s}^{-1}$	Kinematic viscosity of water
ω	0.001	Dimensionless	Parameter controlling nonlinear laminar/turbulent transition
ρ_i	917	$\mathrm{kg\ m}^{-3}$	Bulk density of ice
ρ_w	1000	$\mathrm{kg\ m}^{-3}$	Bulk density of water

Because of the difficulty in accurately constraining b_e to represent englacial storage as water rising in moulins or held in other void spaces in the ice, we assume that this term is negligible compared to the other terms of this equation and eliminate it. This implies that all simulated water is at the bed and we do not attempt to approximate englacial storage, although englacial storage could play an important role in subglacial water flow even in the absence of surface melt (Schoof and others, 2014). The modified water balance equation is then given by

$$\frac{\partial b}{\partial t} + \nabla \cdot \mathbf{q} = \frac{\dot{m}}{\rho_w} + i_{e\to b}. \tag{2}$$

The geometry of the drainage system is represented by the average gap height b over a discrete area of the bed, which evolves through time dynamically. In the original equations, gap height increases as a result of both melt and by sliding over bumps in the bed, and decreases due to creep deformation. This can be expressed as change in gap height over time as

$$\frac{\partial b}{\partial t} = \frac{\dot{m}}{\rho_i} + \beta\,|\mathbf{u}_b| - A|p_i - p_w|^{n-1}(p_i - p_w)b, \tag{3}$$

where ρ_i is the density of ice, β is a dimensionless coefficient that dictates opening of the subglacial gap by sliding over bumps in the bed, $\mathbf{u_b}$ is the ice sliding velocity, A is the flow law parameter, $p_i = \rho_i g H$ is ice overburden pressure in which g is gravitational acceleration and H is ice thickness, $p_w = \rho_w g(h - z_b)$ is subglacial water pressure in which h is hydraulic head and z_b is bed elevation above sea level, and n is Glen's flow law exponent.

The coefficient β that governs opening by sliding over bumps in the bed depends on prescribing an uncertain "typical bed-bump height" (b_r) and "typical bed-bump spacing" (l_r), following Werder and others (2013). This method of cavity opening was introduced by Hewitt (2011) to parameterize an opening mechanism in distributed drainage other than melt, based on the description of linked cavities of Kamb (1987). Schoof and others (2012) found that a system of linked cavities that opened by melt was unstable (assuming turbulent flow); therefore, the opening-by-sliding mechanism has been widely adopted for the evolution of inefficient drainage systems. However, to prevent numerical instability in other models that use this type of opening mechanism, sliding velocity must usually be capped. For example, Poinar and others (2019) applied the Glacier Drainage System model (GlaDS) (Werder and others, 2013) with $b_r = 0.08$ m and $l_r = 2$ m to an idealized Helheim Glacier-like domain, and had to cap sliding speed at 800 m yr^{-1} to achieve model stability. This is an order of magnitude less than observed velocity on Helheim Glacier.

In high-velocity glaciers, including opening by sliding over bumps in SHAKTI effectively smooths out and inhibits any channelized structure, leading to an unrealistic near-uniform gap height equal to the typical bed bump height over large regions. Applying GlaDS to Sermeq Kujalleq (Store Glacier), a tidewater glacier in west Greenland, Cook and others (2020, 2022) selected higher bed bump and spacing values, $b_r = 1$ m and $l_r = 100$ m. This opening mechanism was included in the original SHAKTI equations largely for comparison with other similar models, but is not needed for stability in SHAKTI due to the transitional flux formulation discussed below in Equation 5 and by Sommers and others (2018) that allows for changes between laminar and turbulent flow regimes.

Given how the opening-by-sliding parameterization depends on arbitrarily prescribed bed-bump height and spacing that in reality are heterogeneous, we cannot be confident that the commonly used formulation accurately represents the increase in average b – especially in the case of fast-moving glaciers, which we expect to be underlain by till. We eliminate the "opening by sliding over bumps at the bed" term $\beta\,|\mathbf{u}_b|$ and allow the drainage geometry to open only due to melt, everywhere in the domain, which behaves stably with our transitional flux formulation (Eqn. (5) below). The minimum gap height allowed is 10^{-3} m, representing a transition to premelted films (Wettlaufer and Worster, 2006; Rempel and others, 2022). We write our modified basal gap dynamics equation as

$$\frac{\partial b}{\partial t} = \frac{\dot{m}}{\rho_i} - A|p_i - p_w|^{n-1}(p_i - p_w)b. \tag{4}$$

The momentum equation that describes the water flux is

$$\mathbf{q} = \frac{-b^3 g}{12\nu(1 + \omega Re)}\nabla h, \tag{5}$$

where ν is kinematic viscosity of water, ω is a parameter related to a friction factor that controls the transition from laminar to turbulent flow, and $Re = |\mathbf{q}|/\nu$ is the local Reynolds number. When $\omega Re \ll 1$, Eqn. 5 behaves like laminar flow, with $\mathbf{q}$ proportional to the magnitude of the hydraulic gradient $|\nabla h|$. When $\omega Re \gg 1$, by inserting the definition Re and rearranging to solve for $\mathbf{q}$, we see that $\mathbf{q}$ is proportional to $\sqrt{|\nabla h|}$, corresponding to completely turbulent flow. This flux formulation is based on equations developed in the context of flow in rock fractures (Zimmerman and others, 2004; Chaudhuri and others, 2013; Rajaram and others, 2009). The general Eqn. (5) also allows for intermediate transitional regimes. This flux formulation or "flow law" is the key difference of the original SHAKTI model compared to other subglacial hydrology models, and plays an important role in maintaining stability while allowing for channelization to occur. Forcing $\mathbf{q}$ to be always laminar or always turbulent (by changing the value of ω) results in a model instability in some situations, but these scenarios behave well when allowing for the flexible flow regime transition around $Re = 10^3$ ($\omega = 0.001$), accordingly generating spatially variable Re distributions (Sommers and others, 2018).

In contrast to models that rely on a prescribed hydraulic conductivity, this flux formulation incorporates a spatio-temporally variable hydraulic transmissivity K, given by

$$K = \frac{b^3 g}{12\nu(1 + \omega Re)}. \tag{6}$$

Internal melt generation is represented in SHAKTI through an energy balance at the bed, assuming ice and water are both always at the pressure melting point, i.e.

$$\dot{m}L = G + |\mathbf{u}_b \cdot \tau_b| - \rho_w g\, \mathbf{q} \cdot \nabla h + c_t c_w \rho_w \mathbf{q} \cdot \nabla p_w, \tag{7}$$

where L is the latent heat of fusion of water, G is geothermal heat flux, τ_b is the basal stress, c_t is the change of pressure melting point temperature with pressure, and c_w is the heat capacity of water. This energy equation includes melt due to heat contributed by geothermal sources, frictional heat from sliding over the bed, turbulent dissipation, and adjustments for changes in the pressure melting point due to changes in the water pressure. Note that Equation (9) in Sommers and others (2018) should have a positive sign for the last term as written here in Equation (7), which accounts for changes in the sensible heat due to change in the pressure-melting-point temperature. This term is generally a modest heat sink for flat beds, reducing the melt rate as in Röthlisberger (1972), but can also contribute to enhanced melt with steep slopes or supercooling when flowing uphill in bed overdeepenings (see, e.g. Creyts and Clarke (2010)). This pressure-melt term, however, relies on a problematic assumption that the water pressure and the ice overburden pressure are equal, which is not necessarily true (Clarke, 2005; Wettlaufer and Worster, 2006; Rempel and others, 2022). For this reason, we eliminate this term here.

Basal shear stress as implemented here depends on a drag coefficient C, effective pressure N, and sliding velocity $\mathbf{u_b}$, $\tau_b = C^2 N|\mathbf{u_b}|$. Later, in the Discussion, we examine results using other formulations for τ_b to explore the impact of how frictional heat from sliding is represented. The melt rate at the bed considered here in the reduced form of SHAKTI is a result of geothermal flux, frictional heat from sliding, and heat generated by mechanical energy dissipation in the subglacial system:

$$\dot{m}L = G + |\mathbf{u}_b \cdot \tau_b| - \rho_w g \, \mathbf{q} \cdot \nabla h. \tag{8}$$

We combine equations (2), (4), (5), (6), and (8) to form an elliptic equation in terms of hydraulic head:

$$\nabla \cdot (-K\nabla h) = \dot{m}\left(\frac{1}{\rho_w} - \frac{1}{\rho_i}\right) + A|p_i - p_w|^{n-1}(p_i - p_w)b + i_{e\to b}. \tag{9}$$

We solve Eqn. (9) for the head distribution using a Picard iteration to handle the nonlinear dependence of the terms on the right-hand side of the equation, then we solve Eqn. (4) explicitly to evolve the gap height b. No numerical limits are imposed on head (i.e., water pressure is free to exceed overburden pressure or to become negative over the course of a simulation).

SHAKTI is built into the Ice-sheet and Sea-level System Model (ISSM; Larour and others, 2012) using the finite element method in a parallelized computational framework. In addition to the elimination of terms that rely on uncertain parameters, we modify how the term that describes creep closure in Equation 9 is handled within the Picard iteration. This change helps the Picard iteration converge instead of oscillating, a problem that arises under thick ice with low meltwater input. In previous work with SHAKTI (de Fleurian and others, 2018; Sommers, 2018), this oscillation obstacle was handled using under-relaxation. With a Newton linearization weighting, inspired by Gagliardini and Werder (2018) in their implementation of a similar subglacial hydrology model, GlaDS (Werder and others, 2013) in a different ice-sheet model, Elmer/Ice (Gagliardini and others, 2013), this change to the creep term numerics facilitates convergence of the iterative process to find h. This is a key practical improvement for the application of SHAKTI to glacial environments with thick ice and low water inputs, common in Greenland during the winter.

Model domain

We explore the winter base state subglacial drainage of Helheim Glacier in east Greenland (Figure 1). Helheim is a large, fast-flowing glacier that terminates in Sermilik Fjord with two main branches that flow through deeply incised canyons. We use bed and ice surface elevation based on BedMachine (Morlighem and others, 2017). Our model domain includes the two main branches of Helheim Glacier and extends inland to approximately 1900 m surface elevation. The domain is discretized into an unstructured triangular mesh refined based on ice velocity, with 12,472 finite elements and 6,371 vertices.

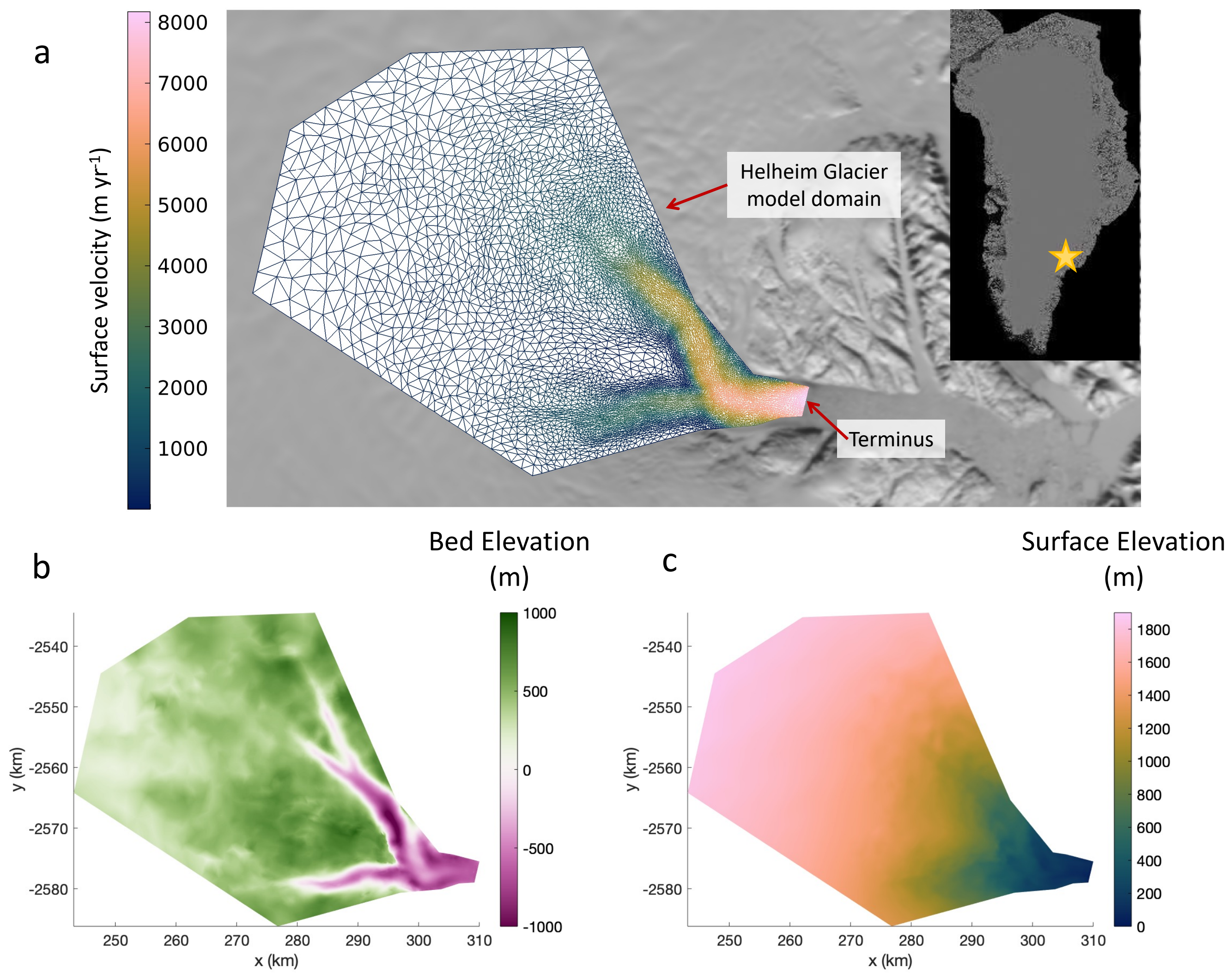

Fig. 1. (a) Location of Helheim Glacier on the Greenland ice sheet (inset), model domain with unstructured mesh used in SHAKTI simulations refined based on surface velocity (Joughin and others, 2018), overlaid on 2010 MODIS mosaic (Haran and others, 2018), (b) bed topography in model domain relative to sea level (Morlighem and others, 2017; Morlighem and et al., 2021), (c) surface elevation in model domain relative to sea level.

Boundary conditions

We set the boundary condition for hydraulic head at the glacier terminus as a Dirichlet condition, based on the idea that the pressure at the subglacial outflow should be equal to hydrostatic pressure from the overlying fjord water (depth varying across the front). Setting the subglacial water pressure equal to the pressure in the fjord at the subglacial outflow gives

$$\rho_w g(h - z_b) = \rho_f g d, \tag{10}$$

where ρ_f is the density of the fjord water and d is the water depth ($d = -z_b$ is a positive quantity, where z_b is bed elevation relative to sea level, i.e. a negative quantity at the terminus). Rearranging, we solve for head:

$$h = \frac{\rho_f}{\rho_w} d + z_b = \left(\frac{\rho_f}{\rho_w} - 1\right) d, \tag{11}$$

where $\rho_f/\rho_w > 1$ and d is a positive quantity. If the water at the subglacial outflow is assumed to be well-mixed with fresh water from melting at the glacier front, then $\rho_w \approx \rho_f$, and therefore $h \approx 0$ at the outflow.

We prescribe Neumann conditions on the upstream and lateral boundaries of the model domain, with $\nabla h = \mathbf{0}$ at these boundaries.

RESULTS

Winter base state

In winter, no surface meltwater is produced, and meltwater inputs that reach the bed from the surface are presumed to be essentially zero over most of the Greenland Ice Sheet. Accordingly, we assume the absence of discrete features (e.g. moulins) or delayed drainage from features such as firn aquifers, in contrast to Poinar and others (2017, 2019). This does not mean, however, that there is no water at the bed in winter, as water is generated at the glacier base (Eqn. 8). Previous work exploring subglacial hydrology on a Helheim-like domain using the GlaDS model invokes a prescribed uniform background basal melt rate (Poinar and others, 2019). To generate an estimate of the winter base state of the subglacial hydrological system of Helheim Glacier, we run a spin-up SHAKTI simulation with zero meltwater input from the englacial system to the bed ($i_{e\rightarrow b} = 0$) with all water at the system produced by basal melt as calculated by Eqn. (8).

In Figure 2, we present the spatial distribution of the subglacial drainage system at the completion of the base state spin-up. In this winter base state with zero external meltwater input, large portions of the bed exhibit high water pressure as demonstrated by a fraction of overburden, p_w/p_i, that is close to one. Distinct preferential drainage pathways emerge with larger gap heights and higher Reynolds numbers forming river-like structures. The major river-like structures coincide with the locations of deeply incised bedrock channels. Effective pressure is highly variable across the domain, lowest near the terminus and lower in the main drainage pathways than in the surrounding bed. Regions of turbulent flow ($Re > 10^3$) as well as regions of laminar flow ($Re < 10^3$) coexist, with clearly higher Re in the main pathways and in smaller arborescent tributaries that feed them. Most of the bed away from the main pathways has very low Re, hence very low flux, with regions that appear to be poorly connected. A clear primary outflow structure emerges at the terminus, located slightly south of the center line. This preferential discharge location agrees well with the location of observed summertime subglacial plumes upwelling at Helheim (Everett and others, 2021; Melton and others, 2022).

Spatially variable transmissivity

In recent years, the community has highlighted the importance of hydraulically isolated and weakly connected regions of the bed in subglacial hydrology, particularly for maintaining observed high winter water pressures (Andrews and others, 2014; Hoffman and others, 2016; Rada and Schoof, 2018; Mejía and others, 2021; Rada Giacaman and Schoof, 2022). An advantage of SHAKTI is that the flux formulation (Eqn. 6) incorporates spatially and temporally variable hydraulic transmissivity, rather than requiring a prescribed value for hydraulic conductivity or transmissivity as in other models. As shown in Figure 3, we find highly heterogeneous transmissivity values, varying over several orders of magnitude within the Helheim domain. Simulated transmissivity is highest near the terminus and along the main winter drainage pathways, and is particularly low along the divide between the two main branches of fast ice flow, as well as through the center of each of these ice streams. The low-transmissivity regions in the center of the main ice flow branches coincide with topographical ridges in the bed, particularly in the northern branch. These low-transmissivity areas represent regions with little connectivity and water flow through them, or in other words are interpreted as poorly connected. In groundwater aquifers, transmissivity of $K < 5$ m^2 d^{-1} is considered to be negligible, $5 < K < 50$ m^2 d^{-1} is weak, $50 < K < 500$ m^2 d^{-1} is moderate, and $K > 500$

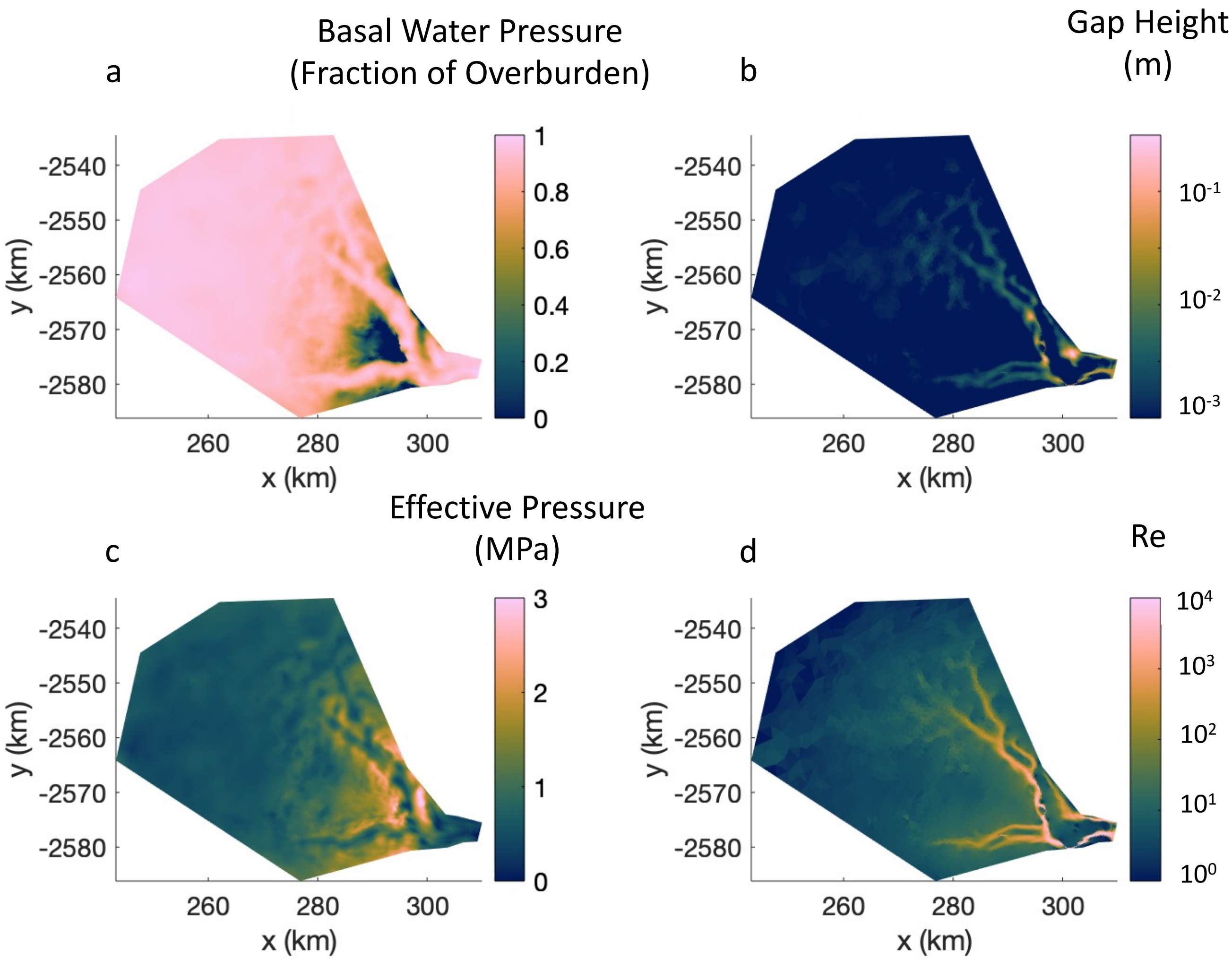

Fig. 2. Winter base state of subglacial hydrological system after spin-up simulation with zero external meltwater input: (a) water pressure as fraction of overburden, p_w/p_i, (b) gap height (shown in $\log_{10}$ scale for detail), (c) effective pressure, (d) Reynolds number (shown in $\log_{10}$ scale for detail).

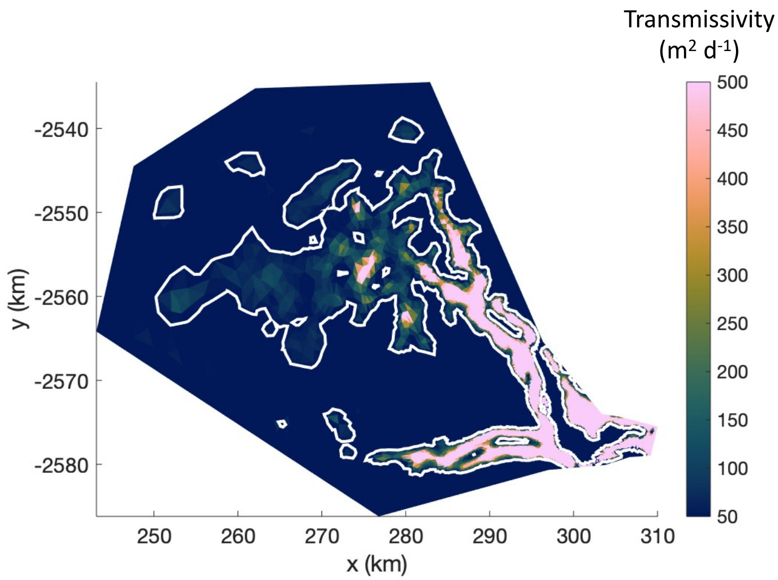

Fig. 3. Winter hydraulic transmissivity (K) as simulated by SHAKTI for Helheim Glacier varies spatially over several orders of magnitude, with high transmissivity near the terminus and through the major river-like drainage pathways, and widespread areas with low transmissivity. The white contour indicates regions with transmissivity of 50 $\mathrm{m^2\ d^{-1}}$, below which is considered to be "weak" transmissivity. The saturated light pink color indicates "high" transmissivity ($K > 500\ \mathrm{m^2\ d^{-1}}$) (De Wiest, 1965).

$\mathrm{m^2\ d^{-1}}$ is high (De Wiest, 1965). Considering the weak transmissivity threshold of $K \leqslant 50\ \mathrm{m^2\ d^{-1}}$ as delineated by the white contour lines in Fig. 3, 71% of the bed by area in our model domain is interpreted to be poorly connected in the winter.

High water pressure in winter

While models have achieved good qualitative behavior for melt-season evolution (Hewitt, 2013; Werder and others, 2013), a challenge of subglacial hydrology modeling has been to reproduce high water pressures in winter conditions to agree with borehole measurements (Flowers, 2015). Disconnected, weakly connected, or isolated regions of the bed have been shown to be necessary for maintaining high winter water pressure (Hoffman and others, 2016; Rada and Schoof, 2019). Our winter SHAKTI simulation of Helheim successfully produces widespread high water pressure (Figure 2) that corresponds with low transmissivity in the interior (Figure 3), suggesting that the flux formulation of SHAKTI (Equation 5) enables representation of winter high-pressure regions with a continuum approach.

The predictions for winter subglacial water pressure in Figure 2 show variability across a range of length scales. Hydropotential flow routing (Shreve, 1972) is commonly used to predict possible subglacial paths. This is typically done by assuming the water pressure to be equal to overburden everywhere ($p_w/p_i = 1.0$), or some other uniform fraction of overburden. However, as shown in Figure 2a, we find that the fraction of overburden varies considerably, spanning the entire range from 0 to 1 over the whole domain, and spanning from ∼0.7–1 in regions of faster ice flow. Assuming a uniform fraction of overburden may thus yield incorrect flowpaths (Wright and others, 2008). In Figure 4, we compare the difference in head distributions from a uniform fraction of overburden and our winter SHAKTI simulation. An assumption of water pressure equal to 100% overburden pressure ($p_w = p_i$, i.e. a uniform fraction of overburden $p_w/p_i = 1.0$) overpredicts the head in the vast majority of the domain, except very near the terminus where it agrees with the results of our SHAKTI simulation. Assuming water pressure equal to 80% overburden pressure ($p_w = 0.8p_i$, i.e. a uniform fraction of overburden $p_w/p_i = 0.8$) agrees better, but still overestimates the head in the more stagnant portions of the domain lateral to the main drainage pathways and underestimates the head near the terminus, in the channels themselves, and further inland regions. Any other assumed uniform fraction of overburden will similarly not account for spatial variations in pressure distribution.

In the presence of steep topographic gradients, as encountered beneath Helheim Glacier, the deeply incised bed topography (and its reflection in surface topography) largely determines the locations of the main drainage paths. Recall that flow is driven by the hydraulic head gradient, and hydraulic head is comprised of two components, pressure head and elevation head: $h = p_w/(\rho_w g) + z_b$. In the case of localized canyons with bed elevation well below sea level, the elevation head in these troughs is sufficiently low to attract water from the surrounding areas, even when the water pressure is higher at the bottom of the canyons. As shown in Figure 4c, the same primary drainage pathways through the deep bed canyons emerge when using a simple routing calculation assuming water pressure equal to 100% overburden everywhere (compare to Re distribution in Figure 2d) . This is true using other uniform fractions of overburden as well, but the configuration of tributary drainage feeding the deep canyons differs. This phenomenon reinforces the necessity of accurate bed topography to predict accurate subglacial flow paths, particularly in places with high-relief mountainous features.

Basal melt

Basal melting has increasingly been acknowledged as an important consideration for ice dynamics (Karlsson and others, 2021; Young and others, 2022). As described in Equation 8, basal meltwater is produced at the

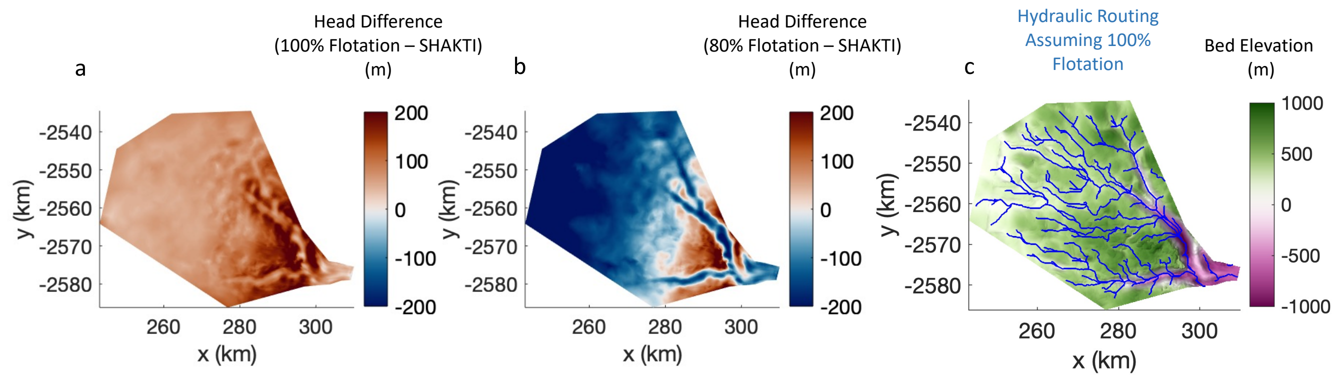

Fig. 4. (a) Difference in hydraulic head between water pressure assumed equal to 100% overburden pressure ($p_w/p_i = 1.0$) and that calculated in our winter SHAKTI simulation. (b) Difference in hydraulic head between water pressure assumed equal to 80% overburden pressure ($p_w/p_i = 0.8$) and our winter SHAKTI simulation. (c) Streamlines based on hydraulic potential flow routing with assumed 100% overburden pressure. The deeply incised bed channels play a major role in determining the location of the main drainage pathways (due to large gradients in elevation head).

bed through geothermal flux, frictional heat from sliding of the ice over the bed, and turbulent dissipation, in which mechanical energy is converted to thermal energy in the water flow. The mean melt rate over the entire domain is 1.2×10^{-5} kg m^{-2} s^{-1} (0.4 m yr^{-1}) and the total melt rate over the domain is 6.3 m^3 s^{-1}. In Figure 5, we present the winter melt rate distribution and the fraction of basal melt rate due to geothermal flux, frictional heat, and dissipation. Geothermal flux is applied in our simulation with a uniform value of 0.05 W m^{-2}, but in reality this varies spatially and may vary by up to a factor of two in narrow incised canyons (Colgan and others, 2021; Willcocks and others, 2021). Frictional heat dominates over most of the domain, yielding the highest melt rates along the steep topographic walls of the deeply incised bed canyons. Dissipation is an important source of basal melt in the faster-flow, higher-melt, river-like structures even in winter.

DISCUSSION

Winter priming of the drainage system

Our winter base state simulation highlights the fact that there is likely widespread subglacial water with non-trivial drainage configurations present year-round under Helheim Glacier, supported by basal meltwater generated by geothermal flux, frictional heat from sliding, and dissipated heat from the water flow, as

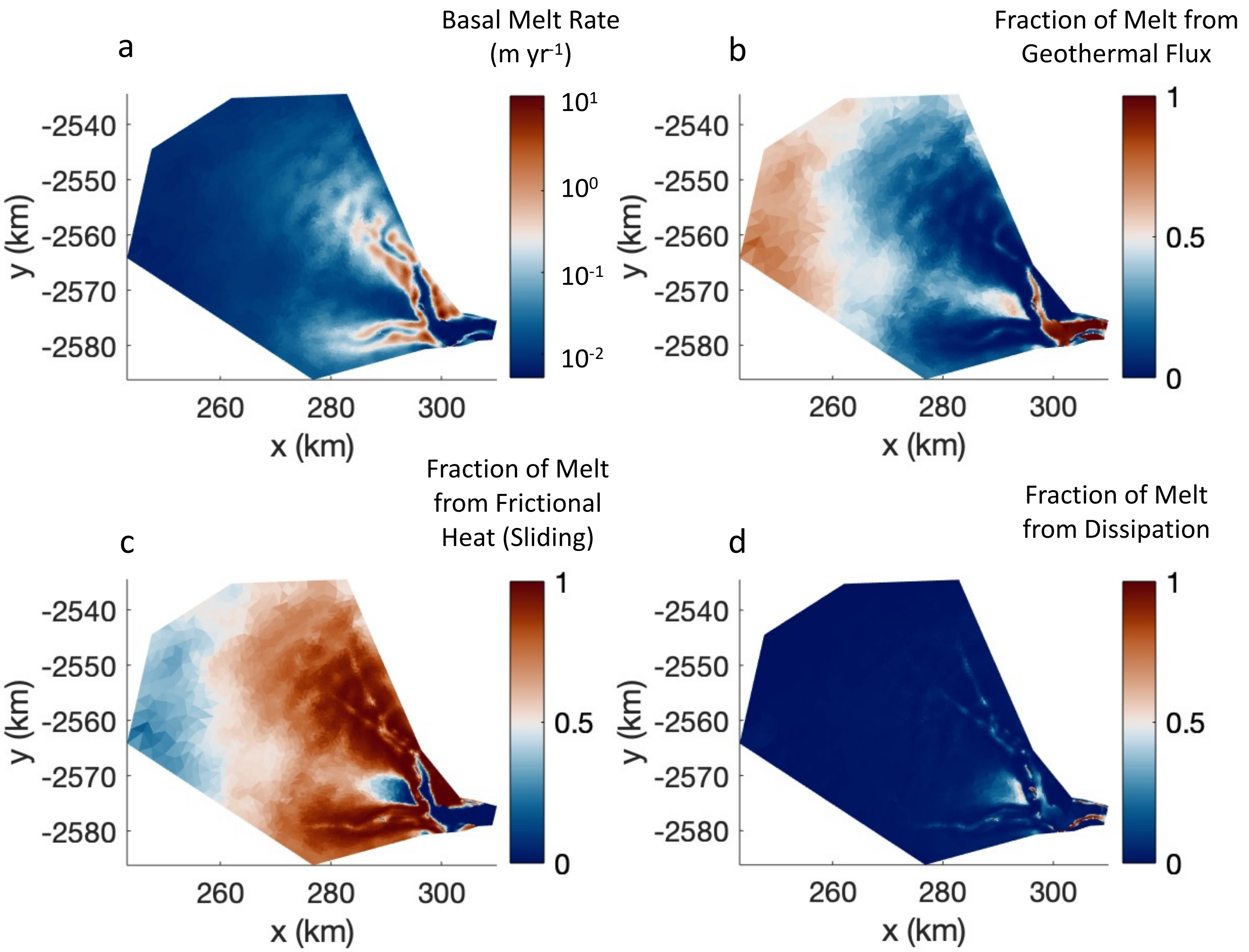

Fig. 5. (a) Total basal melt rate in winter (shown in $\log_{10}$ scale for detail). (b) Fraction of basal melt rate due to geothermal flux. (c) Fraction of basal melt rate due to frictional heat from sliding. (d) Fraction of basal melt rate due to dissipation.

considered here. At Sermeq Kujalleq (Store Glacier), a tidewater glacier in west Greenland, Cook and others (2020) also simulated an active winter subglacial drainage system, bolstered by winter discharge observations (Chauché and others, 2014). Our model results suggest that the drainage system at Helheim does not begin from a totally shut-down state at the initiation of melt each year, but retains some form through the winter. The "deflated" drainage structure without surface meltwater input includes preferential pathways and large areas of low-transmissivity bed, primed to spring into more efficient drainage action with the delivery of surface-generated meltwater to the bed. With our winter simulation results in mind, the seasonal evolution of drainage efficiency and structure may not depend only on the spatio-temporal distribution of moulins and crevasses for meltwater inputs from the surface to the bed (or from englacial drainage of firn aquifers or other storage voids), but is likely also a function of the persistent winter base state drainage structure. Therefore, we recommend considering an existing winter drainage system when interpreting observational data.

Previous work has explored the idea of winter priming beneath the Greenland Ice Sheet. In west Greenland, Chu and others (2016) found water stored on bed ridges in winter, which then flows to depressions and troughs in the melt season. Poinar and others (2019) simulated subglacial hydrology of an idealized Helheim-like glacier (without realistic bed topography) with year-round drainage of firn aquifer water to the bed, finding that increased water at the bed during winter facilitated more rapid and pronounced development of efficient channel networks in the melt season. The winter base state documented here would play a key role in that priming action, and shows that wintertime firn aquifer drainage may not be necessary in order to have year-round channelized structure at Helheim. This is largely because of the deeply incised canyons in the bed that preferentially pull water into river-like features even in the absence of meltwater inputs from the surface or englacial system, and this active winter channelized structure would likely be further enhanced by delayed meltwater drainage from the firn aquifer (Poinar and others, 2017).

River-like winter features

SHAKTI employs a continuum description of subglacial geometry, without distinguishing between different drainage-system components. The way we represent the geometry is through the subglacial gap height b, which is an average of the gap height over an entire element (i.e. generalizing earlier work on spatially lumped models such as Schoof, 2010; Brinkerhoff and others, 2016). This means that SHAKTI does not resolve individual drainage channel geometry by calculating semi-circular cross-sectional area as in some other models (Hewitt, 2013; Werder and others, 2013; Meyer and others, 2016, 2017; Felden and others, 2022). The primary variable sought from subglacial hydrology models for ice dynamics calculations is the subglacial water pressure, which influences sliding velocity. The subglacial water pressure field is relatively smooth compared to small-scale geometric variations (e.g. in gap height) within the subglacial system. Without distinguishing different drainage modes with different evolution equations in each, SHAKTI is able to represent both distributed and channelized sub-systems naturally. With realistic bed topography incorporated, the winter simulation results presented above suggest the promise of SHAKTI in representing weakly connected sub-systems as well. The winter features reminiscent of broad channels have higher water pressure than their surroundings in this winter base state, but lower head, which is what drives the flux of water from the surrounding areas into these pathways due to the deeply incised bed. These river-like features will likely transition with seasonal meltwater input into even more efficient drainage channels.

Role of frictional heat from sliding

Basal melt from frictional heat generated by sliding of the ice over its bed is potentially a dominant source of basal melt, as shown in Fig. 5 and according to basal melt rates for Greenland calculated by Karlsson and others (2021), especially in fast-moving glaciers like Helheim (which moves rapidly even in winter, with winter velocities exceeding 8,000 m yr^{-1}) (Kehrl and others, 2017). However, as discussed by Hansen and Zoet (2022), friction at the ice-bed interface may not be as straightforward as is frequently assumed, and heat may be generated deeper in the basal sediment. To explore the role of frictional heat from sliding in winter base state hydrology, we conduct additional simulations with different formulations for the basal stress τ_b which appears in the melt rate (Equation 8).

In the results presented above, $\tau_b = C^2 N|\mathbf{u_b}|$, where τ_b evolves transiently with N. The drag coefficient, C, is obtained through inverse modeling using ISSM, assuming effective pressure N distribution based on results from a winter spin-up SHAKTI simulation that does not include frictional heat from sliding ($\tau_b = 0$). The inversion optimizes C in order for the ice flow model to reproduce observed surface velocities through the ice stress balance. As we might expect intuitively, the resulting drag coefficient from inversion is high in areas of slow-moving ice (high friction) and low where the ice is sliding rapidly (high slip rates, i.e. in the main glacier branches and near the terminus).

Here, we consider three additional approaches to calculate the basal shear stress τ_b: 1) basal shear stress equal to the driving stress, $\tau_b = \rho_i g H|\nabla z_s|$, 2) a Coulomb-type basal shear stress depending on evolving effective pressure, $\tau_b = 0.3N$, where 0.3 is the till friction coefficient, and 3) zero basal shear stress, $\tau_b = 0$, which effectively removes the influence of frictional heat from sliding.

The resulting winter base state hydrological system differs substantially between these three cases and our original winter simulation. Overall, effective pressure is higher over most of the domain (corresponding to lower water pressure) when frictional heat is included than for the case with $\tau_b = 0$ (Figure 6). Driving stress (blue) and Coulomb-type stress (pink) yield higher basal stress than our original simulation (yellow), and correspondingly lead to higher melt rates. With basal shear stress equal to driving stress or Coulomb-type stress, frictional heat from sliding is the vastly dominant source of basal melt rate over most of the domain and leads to an “over-channelized” drainage system, smoothing out the distinct drainage pathways that emerge in our original simulation and in the absence of frictional heat from sliding (Figure 7). Using the inverted drag coefficient approach in our original simulation, water flux and basal melt rates are high along the walls of the deeply incised bed troughs (Figures 7 and 8). Better defined flow paths are visible than in the other two frictional heat cases, and the drainage regime is distinctly more developed compared to the base state that neglects frictional heat.

We find that subglacial discharge at the terminus varies substantially depending on the frictional heat. Freshwater discharge at the terminus influences melting at the glacier front and mixing in the fjord. In our original simulation, the total outflow is 10.2 m^3 s^{-1}. With no frictional heat from sliding, discharge is lower (2.7 m^3 s^{-1}). With $\tau_b = 0.3N$ and $\tau_b = \rho_i g H |\nabla z_s|$, discharge is several times higher, 130.8 m^3 s^{-1} and 75.8 m^3 s^{-1}, respectively. Similarly, total basal melt rates over the entire domain are affected: 6.3 m^3 s^{-1} in the original simulation, 0.4 m^3 s^{-1} with $\tau_b = 0$, 112.0 m^3 s^{-1} with $\tau_b = 0.3N$, and 65.2 m^3 s^{-1} with $\tau_b = \rho_i g H |\nabla z_s|$.

High localized basal melt rates on the order of 20 m yr^{-1} are calculated when using driving stress or Coulomb-type stress to prescribe basal shear stress (Figure 8), two orders of magnitude higher than the maximum melt rate in the simulation without frictional heat from sliding, 1.0 m yr^{-1}. In our original simulation with $\tau_b = C^2 N u_b$, the maximum local melt rate is 14.4 m yr^{-1} (Figure 8). Whether such high local melt rates are plausible in winter is an interesting question to ponder, as this rate of basal melt is inconsistent with most observations to date. Young and others (2022) inferred basal melt rates of this order of magnitude in west Greenland, but in the context of a summer rain event, not a winter background melt rate. Greenland basal melt rates as calculated by Karlsson and others (2021) are typically < 0.25 m yr^{-1}, which agrees better with the simulation ignoring frictional heat with $\tau_b = 0$. In previous work

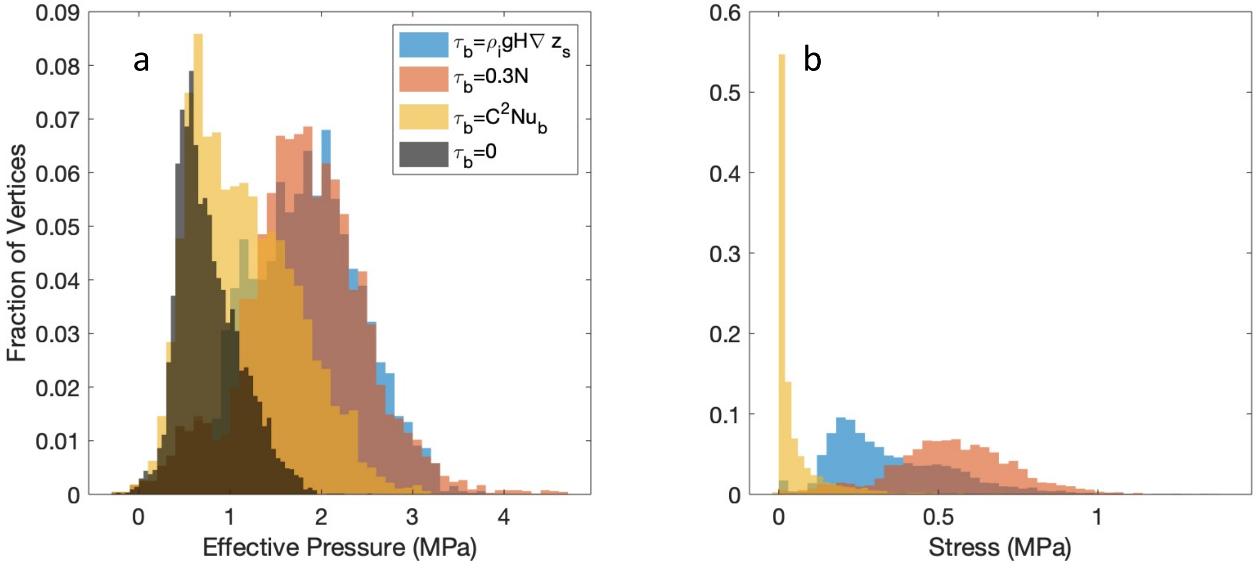

Fig. 6. Histograms comparing different approaches for basal shear stress τ_b: (a) resulting effective pressure distribution, (b) basal shear stress. Including frictional heat from sliding with any of the methods leads to overall higher effective pressure (lower water pressure) than without frictional heat (black). Basal shear stress is significantly higher using the Coulomb-type shear stress $\tau_b = 0.3N$ (pink) or driving stress, $\tau_b = \rho_i g H \nabla z_s$ (blue), compared to that inferred from inverse modeling in ISSM (yellow).

on a Helheim-like idealized glacier, Poinar and others (2019) prescribed a uniform basal melt rate of 0.02 m yr^{-1} (based on thermo-mechanical modeling by Aschwanden and others (2012)). The high melt rates in our simulations are extremely local; the average basal melt rate over a larger area is lower. With high localized basal melt rates included in an ice-dynamics model like ISSM, unusual features may result or the ice would need to compensate by flowing in to fill these melting "sinks".

Given the disparity between the simulation ignoring frictional heat from sliding and the simulations using various formulations for basal shear stress, we demonstrate that frictional heat is an influential control on determining subglacial drainage regimes. We must carefully consider what is likely to be a realistic drainage configuration at Helheim Glacier in the winter. Should we expect widespread high water pressure and clearly defined river-like pathways strongly influenced by the bed topography as we find in the original simulation? Or could there be sufficient heat generated by rapid sliding over the bed so that the water flow is actually more distributed and widespread without distinct river-like features as seen by using driving stress or a Coulomb-type stress for basal shear stress? Including frictional heat from sliding with these latter two methods leads to higher effective pressure (lower water pressure) over most of the interior

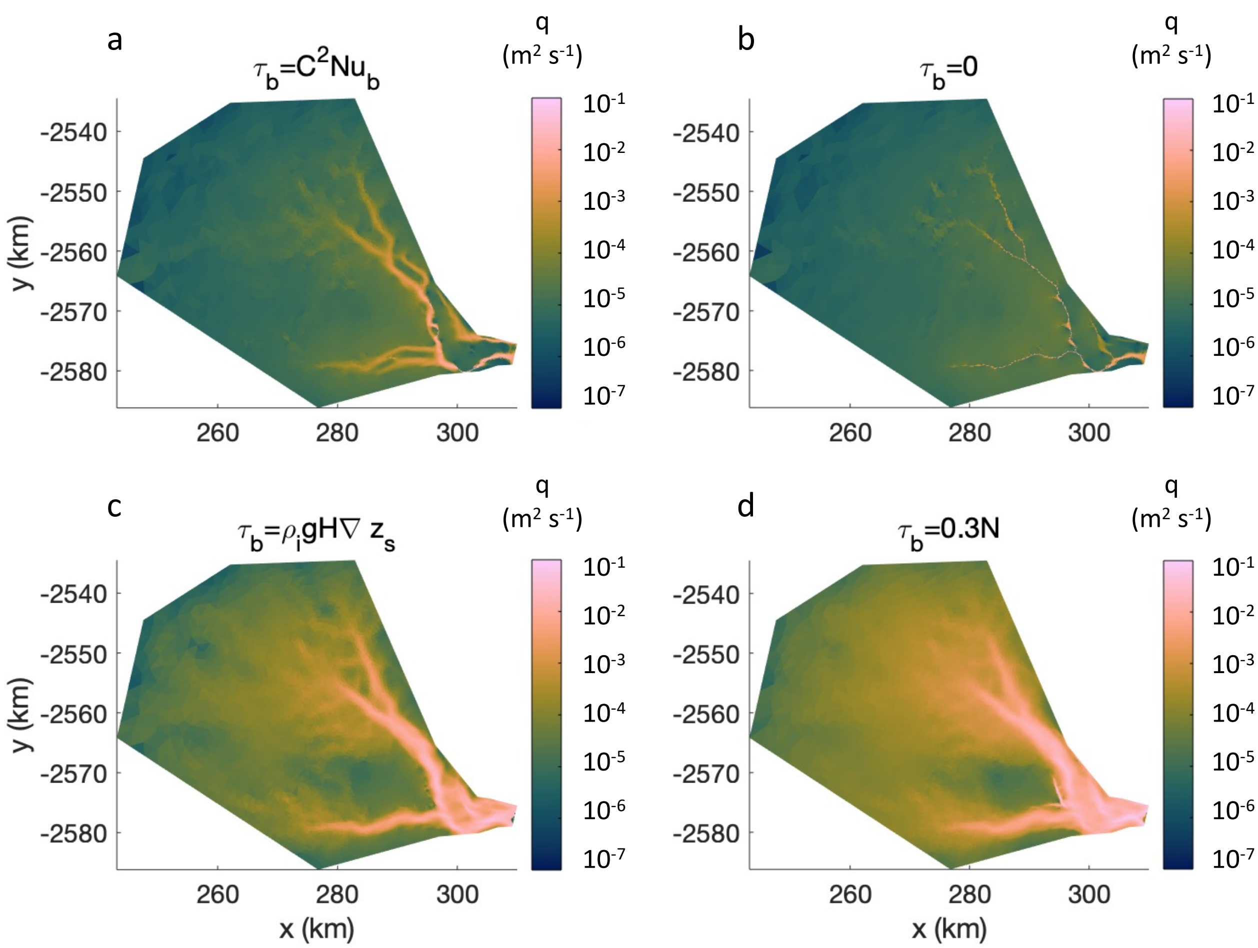

Fig. 7. Winter basal water flux (shown in $\log_{10}$ scale for detail) resulting from different approaches for basal shear stress τ_b: (a) drag coefficient from ISSM inversion, (b) no frictional heat, (c) driving stress, (d) Coulomb-type stress.

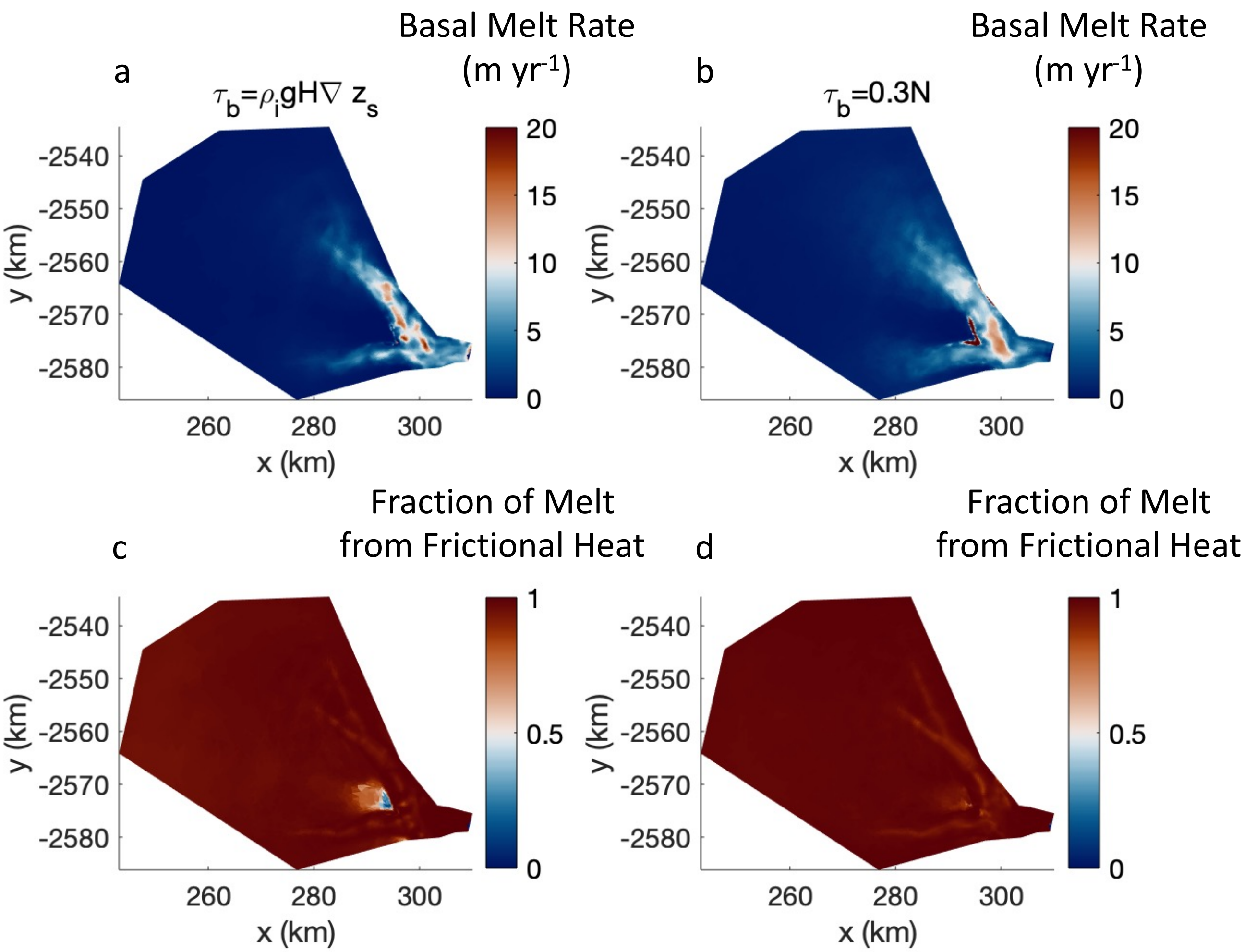

Fig. 8. Basal melt rate with different formulations for basal shear stress: (a) driving stress, (b) Coulomb-type stress. (c) Fraction of melt due to friction heat from sliding with driving stress as basal shear stress, and (d) with Coulomb-type basal shear stress.

domain and increased transmissivity, contrary to our modeling target of reproducing high water pressure in winter. We are encouraged by the success of our original simulation that invokes drag coefficient and friction based on ISSM inversion in producing widespread winter water pressures and poorly connected regions of the bed. In summary, frictional heat from sliding is important in the context of subglacial hydrology in fast-moving glaciers, and should be carefully considered.

Influence of topography

As seen above, the deeply incised bed topography below Helheim Glacier plays a key part in determining the major drainage flow paths. This is due in part to low elevation head and bolstered by high melt rates along the steep walls, primarily attributed to frictional heat. But how much of this river-routing behavior is truly due to the bed topography versus surface slope? To probe sensitivity to bed topography, we consider an additional winter spin-up simulation using modified bed topography, flattening out the bed incisions by raising any bed elevation below sea level ($z_b < 0$) to $z_b = 0$. This effectively reduces the depth of the canyons, in some places by more than 1000 m, and eliminates steep variations in the canyon floors, yielding wide, flat beds beneath the two main ice streams. In simulations with both frictional heat as in our original simulation (using the same drag coefficients from inverse modeling with ISSM) and with no frictional heat, the main subglacial flow paths emerge in similar locations even with the flat-floored canyons. This is likely driven by surface slope (unmodified) in response to underlying bed topography. With the modified flat canyons, however, we calculate reduced overall basal melt rates and lower subglacial discharge at the terminus than with the unmodified BedMachine topography reported above. An important question for further research is to clarify the relationship between bed topography, basal melt rates, and maintenance of the subglacial hydrologic system.

CONCLUSIONS

In this paper, we describe a reduced form of the SHAKTI subglacial hydrology model, retaining only the essential dynamics and parameterizations that do not involve poorly constrained parameters. We demonstrate the utility of SHAKTI through application to a winter base state drainage simulation of Helheim Glacier in east Greenland. Like all models, SHAKTI is an approximation to a complex natural system, paving the way for large-scale coupled simulations.

The main findings are that, with the reduced model, we are able to: (a) reproduce widespread areas of high water pressure in winter using a continuum model, which are widely documented in field measurements and have been difficult to reproduce with subglacial hydrology models, and (b) demonstrate that hydraulic transmissivity as calculated within SHAKTI varies over several orders of magnitude within the domain, naturally representing poorly connected regions of the bed with a continuum approach.

Water pressure as a fraction of overburden varies substantially across the domain, in contrast to a uniform fraction of overburden that is typically assumed in hydropotential routing methods. While spatial pressure variation influences the overall flow configuration, the location of main drainage pathways at Helheim is driven by the deeply incised topographic features in the bed and their corresponding effect in the ice surface slope. Frictional heat from sliding is the dominant source of basal melt rate over much of the domain, yielding high melt rates especially along the steep walls of bed incisions. We also show that dissipation is an important source of melt in the primary river-like drainage pathways that emerge in our winter simulation.

ACKNOWLEDGEMENTS

This study is part of a collaborative project funded by the Heising-Simons Foundation (grants # 2020-1911 (CRM, AS), # 2020-1910 (KP, JM), # 2020-1909 (WC), and #2021-3059 (MM)). SHAKTI is freely available for download as part of the Ice-sheet and Sea-level System Model at https://issm.jpl.nasa.gov/. Model output data and input scripts are available in this Google Drive folder

`https://drive.google.com/drive/folders/1vMpRf_tuaWUYKUTcnI3nqHNVIrVS5f0f?usp=sharing`

and will be made available in a permanent Zenodo archive prior to publication. We are grateful for the Scientific Colour Maps developed by Crameri (2021) and the Arctic Mapping Tools developed by Greene and others (2017).

REFERENCES

Andrews LC, Catania GA, Hoffman MJ, Gulley JD, Lüthi MP, Ryser C, Hawley RL and Neumann TA (2014) Direct observations of evolving subglacial drainage beneath the greenland ice sheet. *Nature*, **514**(7520), 80–83

Aschwanden A, Bueler E, Khroulev C and Blatter H (2012) An enthalpy formulation for glaciers and ice sheets. *Journal of Glaciology*, **58**(209), 441–457

Banwell A, Hewitt I, Willis I and Arnold N (2016) Moulin density controls drainage development beneath the greenland ice sheet. *Journal of Geophysical Research: Earth Surface*, **121**(12), 2248–2269

Brinkerhoff DJ, Meyer CR, Bueler E, Truffer M and Bartholomaus TC (2016) Inversion of a glacier hydrology model. *Ann. Glaciol.*, 1–12 (doi: 10.1017/aog.2016.3)

Chauché N, Hubbard A, Gascard JC, Box JE, Bates R, Koppes M, Sole A, Christoffersen P and Patton H (2014) Ice–ocean interaction and calving front morphology at two west greenland tidewater outlet glaciers. *The Cryosphere*, **8**(4), 1457–1468

Chaudhuri A, Rajaram H and Viswanathan H (2013) Early-stage hypogene karstification in a mountain hydrologic system: A coupled thermohydrochemical model incorporating buoyant convection. *Water Resources Research*, **49**(9), 5880–5899

Chu W, Schroeder DM, Seroussi H, Creyts TT, Palmer SJ and Bell RE (2016) Extensive winter subglacial water storage beneath the greenland ice sheet. *Geophysical Research Letters*, **43**(24), 12–484

Clarke GKC (2005) Subglacial processes. *Annu. Rev. Earth Planet. Sci.*, **33**, 247–276 (doi: 10.1146/annurev.earth.33.092203.122621)

Colgan W, MacGregor JA, Mankoff KD, Haagenson R, Rajaram H, Martos YM, Morlighem M, Fahnestock MA and Kjeldsen KK (2021) Topographic correction of geothermal heat flux in greenland and antarctica. *Journal of Geophysical Research: Earth Surface*, **126**(2), e2020JF005598

Cook SJ, Christoffersen P, Todd J, Slater D and Chauché N (2020) Coupled modelling of subglacial hydrology and calving-front melting at store glacier, west greenland. *The Cryosphere*, **14**(3), 905–924

Cook SJ, Christoffersen P and Todd J (2022) A fully-coupled 3d model of a large greenlandic outlet glacier with evolving subglacial hydrology, frontal plume melting and calving. *Journal of Glaciology*, **68**(269), 486–502

Cowton T, Nienow P, Sole A, Wadham J, Lis G, Bartholomew I, Mair D and Chandler D (2013) Evolution of drainage system morphology at a land-terminating greenlandic outlet glacier. *Journal of Geophysical Research: Earth Surface*, **118**(1), 29–41

Crameri F (2021) Scientific colour maps (7.0.1). *Zenodo*, https://doi.org/10.5281/zenodo.5501399

Creyts TT and Clarke GK (2010) Hydraulics of subglacial supercooling: theory and simulations for clear water flows. *Journal of Geophysical Research: Earth Surface*, **115**(F3)

de Fleurian B, Werder MA, Beyer S, Brinkerhoff DJ, Delaney I, Dow CF, Downs J, Gagliardini O, Hoffman MJ, Hooke RL and others (2018) Shmip the subglacial hydrology model intercomparison project. *Journal of Glaciology*, **64**(248), 897–916

De Wiest RJ (1965) Geohydrology. *Soil Science*, **100**(1), 76

Everett A, Murray T, Selmes N, Holland D and Reeve DE (2021) The impacts of a subglacial discharge plume on calving, submarine melting, and mélange mass loss at helheim glacier, south east greenland. *Journal of Geophysical Research: Earth Surface*, **126**(3), e2020JF005910

Felden AM, Martin DF and Ng EG (2022) Suhmo: an amr subglacial hydrology model v1. 0. *Geoscientific Model Development Discussions*, 1–31

Flowers GE (2015) Modelling water flow under glaciers and ice sheets. *Proceedings of the Royal Society A: Mathematical, Physical and Engineering Sciences*, **471**(2176), 20140907

Fudge T, Humphrey NF, Harper JT and Pfeffer WT (2008) Diurnal fluctuations in borehole water levels: configuration of the drainage system beneath bench glacier, alaska, usa. *Journal of Glaciology*, **54**(185), 297–306

Gagliardini O and Werder MA (2018) Influence of increasing surface melt over decadal timescales on land-terminating greenland-type outlet glaciers. *Journal of Glaciology*, **64**(247), 700–710

Gagliardini O, Zwinger T, Gillet-Chaulet F, Durand G, Favier L, De Fleurian B, Greve R, Malinen M, Martín C, Råback P and others (2013) Capabilities and performance of elmer/ice, a new-generation ice sheet model. *Geoscientific Model Development*, **6**(4), 1299–1318

Greene CA, Gwyther DE and Blankenship DD (2017) Antarctic mapping tools for matlab. *Computers & Geosciences*, **104**, 151–157

Hansen D and Zoet L (2022) Characterizing sediment flux of deforming glacier beds. *Journal of Geophysical Research: Earth Surface*, **127**(4), e2021JF006544

Haran T, Bohlander J, Scambos T, Painter T and Fahnestock M (2018) Measures modis mosaic of greenland (mog) 2005, 2010, and 2015 image maps, version 2. *NASA National Snow and Ice Data Center Distributed Active Archive Center, Boulder, Colorado USA*, 1162–1176

Harper JT, Humphrey NF, Pfeffer WT, Fudge T and O'Neel S (2005) Evolution of subglacial water pressure along a glacier's length. *Annals of Glaciology*, **40**, 31–36

Hewitt I (2013) Seasonal changes in ice sheet motion due to melt water lubrication. *Earth and Planetary Science Letters*, **371**, 16–25

Hewitt IJ (2011) Modelling distributed and channelized subglacial drainage: the spacing of channels. *Journal of Glaciology*, **57**(202), 302–314

Hoffman MJ, Andrews LC, Price SF, Catania GA, Neumann TA, Lüthi MP, Gulley J, Ryser C, Hawley RL and Morriss B (2016) Greenland subglacial drainage evolution regulated by weakly connected regions of the bed. *Nature communications*, **7**(1), 1–12

Iken A, Echelmeyer K, Harrison W and Funk M (1993) Mechanisms of fast flow in jakobshavns isbræ, west greenland: Part i. measurements of temperature and water level in deep boreholes. *Journal of Glaciology*, **39**(131), 15–25

Jordan TM, Williams CN, Schroeder DM, Martos YM, Cooper MA, Siegert MJ, Paden JD, Huybrechts P and Bamber JL (2018) A constraint upon the basal water distribution and thermal state of the greenland ice sheet from radar bed echoes. *The Cryosphere*, **12**(9), 2831–2854

Joughin I, Smith BE and Howat IM (2018) A complete map of greenland ice velocity derived from satellite data collected over 20 years. *Journal of Glaciology*, **64**(243), 1–11

Kamb B (1987) Glacier surge mechanism based on linked cavity configuration of the basal water conduit system. *Journal of Geophysical Research: Solid Earth*, **92**(B9), 9083–9100

Karlsson NB, Solgaard AM, Mankoff KD, Gillet-Chaulet F, MacGregor JA, Box JE, Citterio M, Colgan WT, Larsen SH, Kjeldsen KK and others (2021) A first constraint on basal melt-water production of the greenland ice sheet. *Nature Communications*, **12**(1), 1–10

Kehrl LM, Joughin I, Shean DE, Floricioiu D and Krieger L (2017) Seasonal and interannual variabilities in terminus position, glacier velocity, and surface elevation at helheim and kangerlussuaq glaciers from 2008 to 2016. *Journal of Geophysical Research: Earth Surface*, **122**(9), 1635–1652

Larour E, Seroussi H, Morlighem M and Rignot E (2012) Continental scale, high order, high spatial resolution, ice sheet modeling using the ice sheet system model (issm). *Journal of Geophysical Research: Earth Surface*, **117**(F1)

Mejía J, Gulley J, Trunz C, Covington M, Bartholomaus T, Xie S and Dixon T (2021) Isolated cavities dominate greenland ice sheet dynamic response to lake drainage. *Geophysical Research Letters*, **48**(19), e2021GL094762

Melton SM, Alley RB, Anandakrishnan S, Parizek BR, Shahin MG, Stearns LA, LeWinter AL and Finnegan DC (2022) Meltwater drainage and iceberg calving observed in high-spatiotemporal resolution at helheim glacier, greenland. *Journal of Glaciology*, 1–17

Meyer CR, Fernandes MC, Creyts TT and Rice JR (2016) Effects of ice deformation on Röthlisberger channels and implications for transitions in subglacial hydrology. *J. Glaciol.*, **62**(234), 750–762 (doi: 10.1017/jog.2016.65)

Meyer CR, Hutchinson JW and Rice JR (2017) The path-independent M integral implies the creep closure of englacial and subglacial channels. *J. Appl. Mech.*, **84**(1), 011006 (doi: 10.1115/1.4034828)

Morlighem M and et al (2021) Icebridge bedmachine greenland, version 4 [data set]. *NASA National Snow and Ice Data Center Distributed Active Archive Center*, **https://doi.org/10.5067/VLJ5YXKCNGXO.**

Morlighem M, Williams CN, Rignot E, An L, Arndt JE, Bamber JL, Catania G, Chauché N, Dowdeswell JA, Dorschel B and others (2017) Bedmachine v3: Complete bed topography and ocean bathymetry mapping of greenland from multibeam echo sounding combined with mass conservation. *Geophysical research letters*, **44**(21), 11–051

Murray T and Clarke GK (1995) Black-box modeling of the subglacial water system. *Journal of Geophysical Research: Solid Earth*, **100**(B6), 10231–10245

Nienow P, Sharp M and Willis I (1998) Seasonal changes in the morphology of the subglacial drainage system, haut glacier d'arolla, switzerland. *Earth Surface Processes and Landforms: The Journal of the British Geomorphological Group*, **23**(9), 825–843

Oswald G and Gogineni S (2008) Recovery of subglacial water extent from greenland radar survey data. *Journal of Glaciology*, **54**(184), 94–106

Oswald GK, Rezvanbehbahani S and Stearns LA (2018) Radar evidence of ponded subglacial water in greenland. *Journal of Glaciology*, **64**(247), 711–729

Poinar K, Joughin I, Lilien D, Brucker L, Kehrl L and Nowicki S (2017) Drainage of southeast greenland firn aquifer water through crevasses to the bed. *Frontiers in Earth Science*, **5**, 5

Poinar K, Dow CF and Andrews LC (2019) Long-term support of an active subglacial hydrologic system in southeast greenland by firn aquifers. *Geophysical Research Letters*, **46**(9), 4772–4781

Rada C and Schoof C (2018) Channelized, distributed, and disconnected: subglacial drainage under a valley glacier in the yukon. *The Cryosphere*, **12**(8), 2609–2636

Rada C and Schoof C (2019) The role of hydraulically disconnected areas on basal sliding: Insights from small alpine glacier on the st. elias range, yukon territory, canada. In *AGU Fall Meeting Abstracts*, volume 2019, C13C–1323

Rada Giacaman CA and Schoof C (2022) Channelised, distributed, and disconnected: Spatial structure and temporal evolution of the subglacial drainage under a valley glacier in the yukon. *The Cryosphere Discussions*, 1–39

Rajaram H, Cheung W and Chaudhuri A (2009) Natural analogs for improved understanding of coupled processes in engineered earth systems: examples from karst system evolution. *Current Science*, 1162–1176

Rempel AW, Meyer CR and Riverman KL (2022) Melting temperature changes during slip across subglacial cavities drive basal mass exchange. *J. Glaciol.*, **68**(267), 197–203 (doi: 10.1017/jog.2021.107)

Röthlisberger H (1972) Water pressure in intra-and subglacial channels. *Journal of Glaciology*, **11**(62), 177–203

Ryser C, Lüthi MP, Andrews LC, Catania GA, Funk M, Hawley R, Hoffman M and Neumann TA (2014a) Caterpillar-like ice motion in the ablation zone of the greenland ice sheet. *Journal of Geophysical Research: Earth Surface*, **119**(10), 2258–2271

Ryser C, Lüthi MP, Andrews LC, Hoffman MJ, Catania GA, Hawley RL, Neumann TA and Kristensen SS (2014b) Sustained high basal motion of the greenland ice sheet revealed by borehole deformation. *Journal of Glaciology*, **60**(222), 647–660

Schoof C (2010) Ice-sheet acceleration driven by melt supply variability. *Nature*, **468**(7325), 803–806

Schoof C, Hewitt IJ and Werder MA (2012) Flotation and free surface flow in a model for subglacial drainage. part 1. distributed drainage. *Journal of Fluid Mechanics*, **702**, 126–156

Schoof C, Rada C, Wilson N, Flowers G and Haseloff M (2014) Oscillatory subglacial drainage in the absence of surface melt. *The Cryosphere*, **8**(3), 959–976

Shreve R (1972) Movement of water in glaciers. *Journal of Glaciology*, **11**(62), 205–214

Sommers A, Rajaram H and Morlighem M (2018) Shakti: subglacial hydrology and kinetic, transient interactions v1. 0. *Geoscientific Model Development*, **11**(7), 2955–2974

Sommers AN (2018) *Insights into Processes Affecting Greenland Ice Sheet Dynamics in a Changing Climate: Firn Permeability, Interior Thermal State, Subglacial Hydrology, and Heat Transfer Coefficients*. Ph.D. thesis, University of Colorado at Boulder

Werder MA, Hewitt IJ, Schoof CG and Flowers GE (2013) Modeling channelized and distributed subglacial drainage in two dimensions. *Journal of Geophysical Research: Earth Surface*, **118**(4), 2140–2158

Wettlaufer JS and Worster MG (2006) Premelting dynamics. *Annu. Rev. Fluid Mech.*, **38**(1), 427–452 (doi: 10.1146/annurev.fluid.37.061903.175758)

Willcocks S, Hasterok D and Jennings S (2021) Thermal refraction: implications for subglacial heat flux. *Journal of Glaciology*, **67**(265), 875–884

Wright A, Siegert M, Le Brocq A and Gore D (2008) High sensitivity of subglacial hydrological pathways in antarctica to small ice-sheet changes. *Geophysical Research Letters*, **35**(17)

Young TJ, Christoffersen P, Bougamont M, Tulaczyk SM, Hubbard B, Mankoff KD, Nicholls KW and Stewart CL (2022) Rapid basal melting of the greenland ice sheet from surface meltwater drainage. *Proceedings of the National Academy of Sciences*, **119**(10), e2116036119

Zimmerman RW, Al-Yaarubi A, Pain CC and Grattoni CA (2004) Non-linear regimes of fluid flow in rock fractures. *International Journal of Rock Mechanics and Mining Sciences*, **41**, 163–169